Optical third harmonic generation in the magnetic semiconductor EuSe

M. Lafrentz,[1] D. Brunne,[1] B. Kaminski,[1] V. V. Pavlov,[2] R. V. Pisarev,[2] A. B. Henriques,[3] D. R. Yakovlev,[1,2]
G. Springholz,[4] G. Bauer,[4] and M. Bayer[1]

[1]*Experimentelle Physik 2, Technische Universität Dortmund, D-44221 Dortmund, Germany*
[2]*Ioffe Physical-Technical Institute, Russian Academy of Sciences, 194021 St. Petersburg, Russia*
[3]*Instituto de Física, Universidade de São Paulo, 05315-970 São Paulo, Brazil*
[4]*Institut für Halbleiter- und Festkörperphysik, Johannes Kepler Universität Linz, A-4040 Linz, Austria*

(Received 2 November 2011; revised manuscript received 21 December 2011; published 17 January 2012)

Third harmonic generation (THG) has been studied in europium selenide EuSe in the vicinity of the band gap at 2.1–2.6 eV and at higher energies up to 3.7 eV. EuSe is a magnetic semiconductor crystalizing in centrosymmetric structure of rock-salt type with the point group $m3m$. For this symmetry the crystallographic and magnetic-field-induced THG nonlinearities are allowed in the electric-dipole approximation. Using temperature, magnetic field, and rotational anisotropy measurements, the crystallographic and magnetic-field-induced contributions to THG were unambiguously separated. Strong resonant magnetic-field-induced THG signals were measured at energies in the range of 2.1–2.6 eV and 3.1–3.6 eV for which we assign to transitions from $4f^7$ to $4f^6 5d^1$ bands, namely involving $5d(t_{2g})$ and $5d(e_g)$ states.

DOI: 10.1103/PhysRevB.85.035206 PACS number(s): 75.50.Pp, 42.65.Ky

I. INTRODUCTION

For many years the magnetic semiconductors EuX (X = O, S, Se, and Te) have attracted interest due to their unique physical properties. Their transport, magnetic, and magneto-optical properties are determined by strongly localized $4f^7$ electrons of Eu^{2+} ions with spin $S = 7/2$.[1–3] Most of the early research in the 1960s and 1970s were performed on bulk single crystals and noncrystalline thin films of EuX. However, during the last decade high quality epitaxial thin films were successfully grown on Si and GaN semiconductor substrates, which opened new opportunities for applications of these materials.[4,5] For example, EuO has been suggested for spin-filter devices,[6–10] and EuS,[11–17] as well as EuSe (Ref. 18) for tunnel junctions.

Nonlinear magneto-optical properties of EuX remained unexplored until recent studies on optical harmonics generation.[19–23] Using second harmonic generation (SHG) a novel type of nonlinear optical susceptibility was discovered in EuTe and EuSe.[19] Spatially resolved SHG in EuO films disclose a submicron size of ferromagnetic domains.[22] When both SHG and third harmonic generation (THG) processes are allowed in the same medium they can provide complementary information on crystallographic, electronic, and magnetic structures. It should be noted that THG spectroscopic studies[21] have been performed much more seldom than SHG ones.[19,24–26]

In this paper we report on a spectroscopic study of crystallographic and magnetic-field-induced THG in the magnetic semiconductor EuSe. We found that in EuSe the THG is strongly enhanced in the vicinity of the band gap at 2.1–2.6 eV and for several other resonances at higher energies. Strong magnetic-field-induced contributions to the THG spectra were revealed by temperature, magnetic field, and rotational anisotropy studies.

The paper is organized as follows. Section II briefly summarizes the details of the experimental technique and properties of the investigated EuSe samples. Section III gives the phenomenological description of crystallographic and magnetic-field-induced THG in EuSe. Experimental results and discussion are presented in Sec. IV.

II. SAMPLES AND EXPERIMENTAL TECHNIQUE

The THG experiments were performed on (111)-oriented EuSe layers grown by molecular-beam epitaxy. The EuSe epilayers of 0.5 μm thickness were grown on BaF_2 substrates and capped with a 40-nm-thick (111) BaF_2 protective layer. With a band gap of about 9.2 eV BaF_2 is fully transparent in the spectral region of interest for our study. Measurements on pure BaF_2 substrate showed no THG signals in this region. X-ray analysis confirmed high structural quality. The EuSe layer is nearly lattice matched to BaF_2, so the magnetic phase diagram should not be affected by strain.[27] The EuSe crystallographic structure has rock-salt symmetry with the centrosymmetric point group $m3m$ (O_h).[20] The face-centered-cubic lattice contains a two-atom basis with an Eu^{2+} ion at (1/2,1/2,1/2) and a Se^{2-} ion at (0,0,0). The divalent Eu^{2+} ions are octahedrally surrounded by six Se^{2-} ions forming a strong ionic binding, which results in empty $5d$ states of europium and completely filled p orbitals of selenium. The high quality EuSe epitaxial films used in this work allowed us to study THG in a wide spectral range up to 3.7 eV.

The magnetic properties of EuSe are determined by the ground state of the Eu^{2+} ions in which the $4f^7$ electrons with spin $S = 7/2$ are involved.[1,28,29] EuSe can be classified as Heisenberg magnet with two competing interactions: the nearest-neighbor ferromagnetic exchange integral J_1 and the next-nearest-neighbor antiferromagnetic exchange integral J_2. Ratios of the J_1 and J_2 integrals and their competition with an external magnetic field result in a complicated magnetic phase diagram including antiferromagnetic (AFM), ferrimagnetic (FIM), and ferromagnetic (FM) ordering, as well as a paramagnetic phase at elevated temperatures.[1,27] EuSe is metamagnetic with $T_N = 4.6$ K and shows a mixed AFM and FIM ordering below 2.8 K.

THG was studied in transmission geometry using the experimental technique described in Refs. 21 and 25. A tunable

type-II optical parametric oscillator (OPO) pumped by the third harmonic (3.49 eV) of a solid-state Nd:YAG laser was used as a source of fundamental light in a wide spectral range. The laser system generates pulses of 8 ns duration at 10 Hz repetition rate with a typical pulse power of 15–60 mJ and a linewidth of about 0.5 meV. The pulse power at the sample was about 3–5 mJ. The required laser light polarization at the fundamental frequency was set by a Glan-Thomson prism and a half-wavelength plate. The resulting THG signal was analyzed by polarization optics, filtered by a spectrometer and detected by a cooled charge-coupled-device camera. The sample temperature T was varied from 1.6 to 150 K. External magnetic fields $\mathbf{B}$ up to 2 T were applied in the Voigt geometry, perpendicular to both the EuSe layer growth axis [111] and the light wave vector.

III. CRYSTALLOGRAPHIC AND MAGNETIC-FIELD-INDUCED CONTRIBUTIONS TO THG

Among different nonlinear optical phenomena related with frequency conversion the third harmonic generation is the simplest process that is allowed in the electric-dipole (ED) approximation for any media. By contrast ED-SHG is only allowed in noncentrosymmetric media. The relevant THG crystallographic (CED) nonlinear polarization $\mathbf{P}^{\mathrm{CED}}(3\omega)$ can be written as[30,31]

$$P_i^{\mathrm{CED}}(3\omega) = \chi^{(3)}_{ijkl}(3\omega)E_j(\omega)E_k(\omega)E_l(\omega), \qquad (1)$$

where $\chi^{(3)}_{ijkl}(3\omega)$ is the third-order nonlinear optical susceptibility being responsible for the crystallographic contributions to THG. $E_{j,k,l}(\omega)$ are the fundamental optical fields. The THG process described by a polar fourth-rank tensor $\chi^{(3)}_{ijkl}$ is allowed in materials of any symmetry.[30–33] Its relevant nonvanishing tensor components can be found in Refs. 21,32 and 33.

In general, THG, being controlled by a higher-order nonlinear susceptibility, extends significantly the application range of the nonlinear spectroscopy.[21] In materials without space-inversion symmetry the THG susceptibilities are smaller in magnitude than ED-SHG nonlinearities, and in this case THG serves rather as a complimentary tool. However, THG spectroscopy is really powerful for investigating materials where ED-SHG is forbidden. The strong enhancement of susceptibility in the vicinity of electronic resonances can provide larger THG intensities, too. Further, THG allows studies of hidden symmetries, which are modified by phase transitions or broken by external fields via the interplay of high-order nonlinearities.[34]

Recent experimental studies of SHG in EuTe and EuSe,[19,20] and THG in EuTe,[21] have shown that a ferromagnetic component of the magnetic structure and a magnetic-field-induced magnetization are responsible for the magnetic-field-induced nonlinearities. In the ED approximation the magnetic-field-induced (IED) nonlinear polarization $\mathbf{P}_i^{\mathrm{IED}}(3\omega)$ can be written as

$$P_i^{\mathrm{IED}}(3\omega) = \chi^{(4)}_{ijklm}(3\omega)E_j(\omega)E_k(\omega)E_l(\omega)M_m(0), \qquad (2)$$

where THG susceptibility $\chi^{(4)}_{ijklm}(3\omega)$ is an axial fifth-rank tensor,[32] and $M_m(0)$ is a component of an axial magnetization vector. Below the Néel temperature T_{N}, this vector coincides with the spontaneous or induced ferromagnetic vector for AFM, FIM, and FM ordering. In the paramagnetic phase above T_{N} the vector $\mathbf{M}$ corresponds to the magnetization induced by the external magnetic field. Within the ED approximation this magnetic-field-induced contribution to THG is allowed in crystals of any symmetry, since the presence of $M_m(0)$ does not break the inversion symmetry. The nonvanishing tensor components of $\chi^{(4)}_{ijklm}$ can be found in Refs. 21 and 32.

The resulting THG intensity, taking into account both crystallographic and magnetic-field-induced nonlinear polarizations, can be written as

$$I(3\omega) \propto |\mathbf{P}^{\mathrm{CED}}|^2 + |\mathbf{P}^{\mathrm{IED}}|^2 \pm 2|\mathbf{P}^{\mathrm{CED}}||\mathbf{P}^{\mathrm{IED}}|\cos\phi, \qquad (3)$$

where ϕ denotes a phase difference between CED and IED contributions. The first term in Eq. (3) is a pure crystallographic contribution. The second term is a pure magnetic-field-induced contribution, which is proportional to $\mathbf{M}^2$. The third interference term is proportional to the axial vector $\mathbf{M}$, where $\pm$ signs refer to opposite orientations of $\mathbf{M}$. Neglecting energy dissipation in the medium one can show that $\chi^{(3)}_{ijkl}$ is a real tensor, $\chi^{(4)}_{ijklm}$ is a pure imaginary tensor, and the interference term vanishes when $\phi = \pi/2$. In the case of energy dissipation or the presence of resonance states the interference term can appear similar to the interference of crystallographic and magnetic contributions in the SHG process.[24,35]

IV. EXPERIMENTAL RESULTS AND DISCUSSION

Figure 1 shows THG spectra of EuSe recorded for polarization geometries $\mathbf{E}(3\omega) \parallel \mathbf{E}(\omega)$ and $\mathbf{E}(3\omega) \perp \mathbf{E}(\omega)$ at $T = 1.6$ K in the absence of an external magnetic field. In the wide spectral range from 2.0 up to 3.7 eV two broad bands centered around 2.2 and 3.4 eV are observed. The THG spectrum in EuSe is qualitatively similar to the same spectrum in EuTe, where also two bands separated by about 1 eV are detected.[21] Obviously, the electronic band structure of the europium chalcogenides is of key importance for understanding their nonlinear optical properties. Its relation with the microscopic model for the THG in EuTe was thoroughly discussed in Ref. 21. In the vicinity of the band gap of europium chalcogenides the electronic structure is controlled by the levels of Eu^{2+} ions, and therefore it is similar in EuTe and EuSe. From the energy positions of the THG bands in Fig. 1 we assign the low-energy 2.2-eV band to $4f^7 \rightarrow 4f^6 5d^1(t_{2g})$ electronic transitions, and the high-energy 3.4-eV band to $4f^7 \rightarrow 4f^6 5d^1(e_g)$ transitions.[38] The energy separation of 1.2 eV between the t_{2g} and e_g THG bands in EuSe is larger by ~0.4 eV than the energy separation between the two THG bands seen in EuTe, which is explained by the larger crystal-field splitting in EuSe in comparison to the same splitting in EuTe.[36] Intensity and spectral shape of the THG signals do not depend on the temperature in the range 1.6–50 K; see inset in Fig. 1.

The isotropic angle distribution of THG intensity for $\mathbf{E}(3\omega) \parallel \mathbf{E}(\omega)$ shown in the inset of Fig. 1 is in agreement with the phenomenological considerations leading to Eq. (1). For $\mathbf{E}(3\omega) \perp \mathbf{E}(\omega)$ configuration the THG signal is not expected within the electric-dipole approximation. Only a very weak

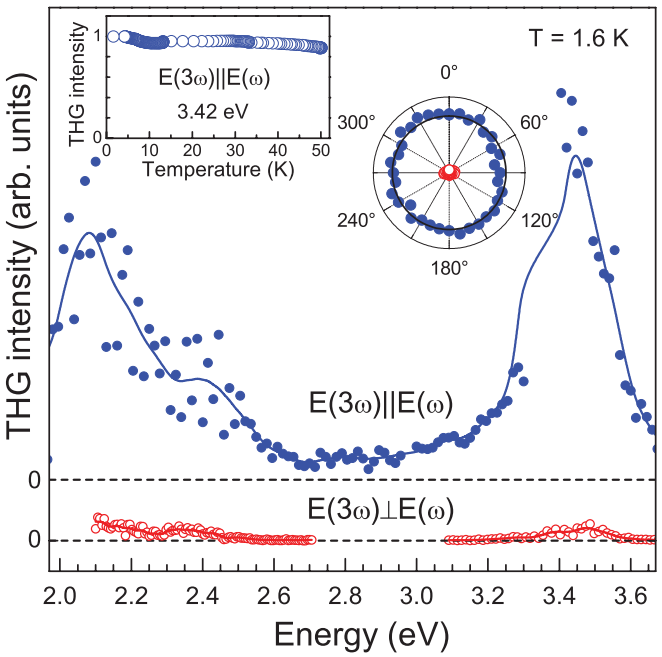

FIG. 1. (Color online) THG spectra of EuSe for two experimental geometries. Solid lines give a guide for the eye and dashed lines indicate zero level. Insets show the temperature and angular dependences of the THG intensity at $E(3\omega) = 3.42$ eV; the latter is measured at $T = 1.6$ K. In the rotational diagram the symbol color indicates the configuration: blue closed circles located in vicinity of black solid line represent $\mathbf{E}(3\omega) \parallel \mathbf{E}(\omega)$ and red open circles in the very center represent $\mathbf{E}(3\omega) \perp \mathbf{E}(\omega)$.

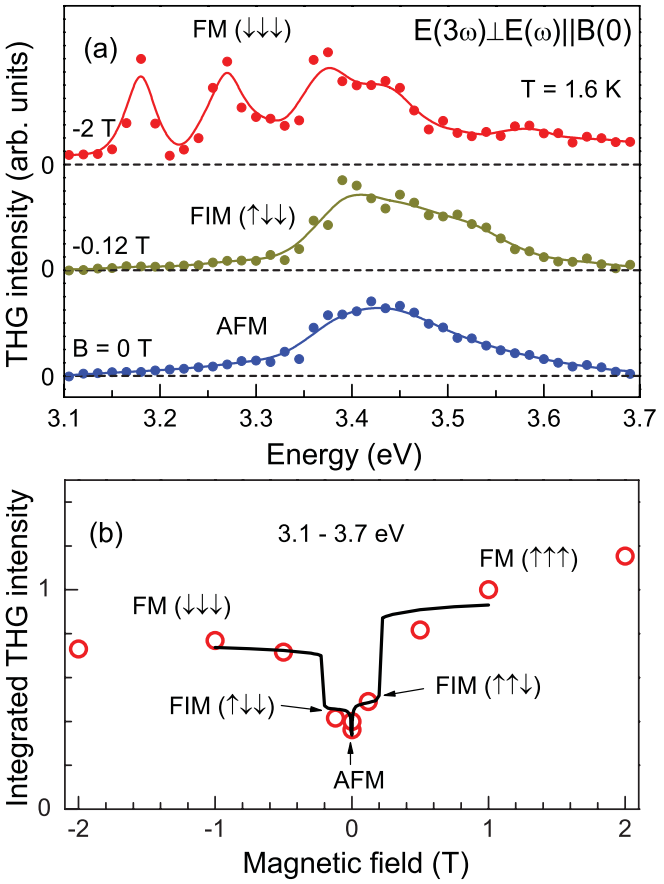

FIG. 2. (Color online) (a) THG spectra of EuSe in the range 3.1–3.7 eV measured in $\mathbf{E}(3\omega) \perp \mathbf{E}(\omega) \parallel \mathbf{B}(0)$ configuration in different magnetic fields. Solid lines give a guide for the eye and dashed lines indicate zero level. (b) The open circles show the magnetic-field dependence of the THG intensity integrated over the spectral range 3.1–3.7 eV. The solid line gives normalized $[a + bM(B)]^2$ dependence with $a \approx 1.3b$ and $M(B)$ after Ref. 27.

intensity of a residual signal of about 1% stemming from CED contribution is observed in the perpendicular configuration, which may come out from the leak of the parallel configuration. Finally, rotational diagrams and temperature dependence lead us to conclude that in the absence of external magnetic fields the strong THG signal for the $\mathbf{E}(3\omega) \parallel \mathbf{E}(\omega)$ configuration has no magnetic contribution; it is rather controlled by crystallographic ones.

In order to study the magnetic-field-induced THG signals one should focus on the $\mathbf{E}(3\omega) \perp \mathbf{E}(\omega)$ configuration, where CED is absent in the electric-dipole approximation. Figure 2(a) shows THG spectra of the high-energy band associated with $4f^7 \rightarrow 4f^6 5d^1(e_g)$ transitions in different magnetic fields. Changing the magnetic-field strength switches EuSe between different magnetic phases. In the FIM phase at $B = -0.12$ T the observed THG spectrum does not change significantly compared to the AFM phase at $B = 0$. In contrast, in the FM phase two new pronounced features appear at 3.18 and 3.27 eV reflecting the complicated structure of the excited state $f^6 5d^1(e_g)$.[21]

Figure 2(b) shows the integrated intensity in the spectral range 3.1–3.7 eV. In the FIM phase the integral THG intensity increases slightly. In the FM phase it increases further reaching a saturation level for $|B| > 1$ T. It is already known from a Faraday effect study,[37] that in EuSe the internal alignment of spins reaches 80% of its saturation value at magnetic fields of about 1 T and it is only weakly increased in higher fields up to 7 T. A good approximation for this behavior can be achieved by a dependence $[a + bM(B)]^2$ with $a \approx 1.3b$ and $M(B)$ after Ref. 27. The nearly equal values of a and b demonstrate that in the perpendicular configuration the IED and the residual CED THG intensities are of the same order.

Figure 3 depicts the magnetic-field behavior for the lower energy THG band assigned to $4f^7 \rightarrow 4f^6 5d^1(t_{2g})$ transitions. At zero magnetic field there is a small CED contribution in the AFM phase. In the FIM phase the new distinct feature appears at 2.35 eV, which can be attributed to the IED contribution. This contribution increases further with growing field and saturates for the FM phase; see inset of Fig. 3.

Figure 4 shows representative THG rotational anisotropies recorded in a magnetic field of -0.5 T at $E(3\omega) = 3.27$ eV for parallel and perpendicular polarization geometries. For the parallel polarization geometry the isotropic diagram is distorted by an elongation parallel and perpendicular to the orientation of the external magnetic field. For the perpendicular polarization geometry the rotational diagram has a pronounced fourfold symmetry. This is in agreement with the symmetry considerations for the CED and IED contributions accounting for their interference; see Eqs. (1)–(3). We would like to remind that in the absence of external magnetic field the CED contribution of THG signal has isotropic rotational anisotropy;

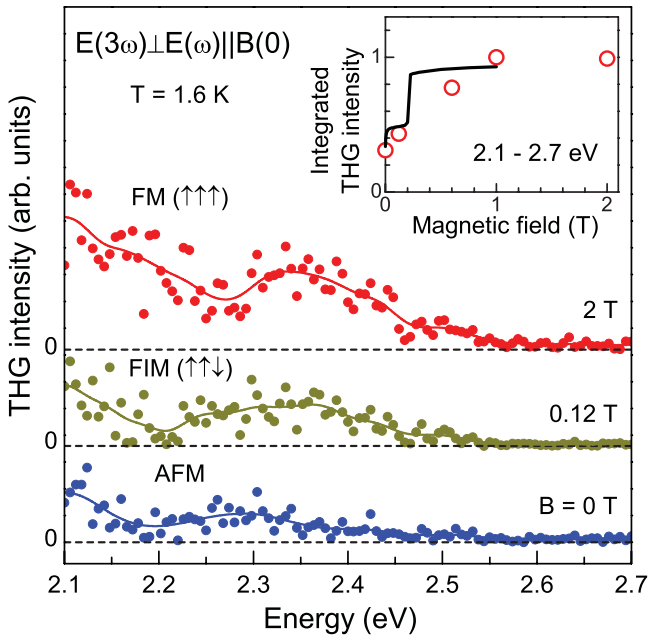

FIG. 3. (Color online) THG spectra of EuSe in the range 2.1–2.7 eV measured in different magnetic fields. Solid lines give a guide for the eye and dashed lines indicate zero level. The inset shows the magnetic-field dependence of the THG intensity (open circles) integrated over the spectral range 2.1–2.7 eV. Normalized dependence $[a + bM(B)]^2$, same as in Fig. 2(b), is shown by a solid line.

see inset in Fig. 1. Therefore the magnetic-field-induced changes in the pattern of the rotational anisotropy shown in Fig. 4 highlight the role of the magnetic contribution to the THG signal measured in external magnetic fields.

Figure 5 shows THG spectra of EuSe at different temperatures measured in the range 3.1–3.7 eV for $4f^7 \rightarrow 4f^6 5d^1(e_g)$ transitions. The polarization configuration is $\mathbf{E}(3\omega) \perp \mathbf{E}(\omega)$ and $B = -2$ T. One can see that the increase of the lattice temperature from 1.6 to 145 K modifies significantly the THG spectra and their integral intensity. Bands at 3.18 and 3.27 eV decrease in intensity and shift to higher energies with the temperature increase from 1.6 to 6 K, and completely disappear at temperatures exceeding 13 K. Such a behavior is typical for magnetic-field-induced contributions. In contrast,

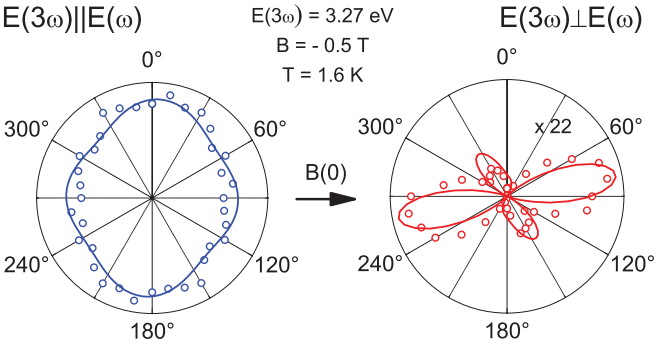

FIG. 4. (Color online) THG rotational anisotropies for $\mathbf{E}(3\omega) \parallel \mathbf{E}(\omega)$ and $\mathbf{E}(3\omega) \perp \mathbf{E}(\omega)$ geometries. Open circles show measured data and solid lines represent best fits performed with the use of Eq. (3) and also Eqs. (10) and (11) from Ref. 21.

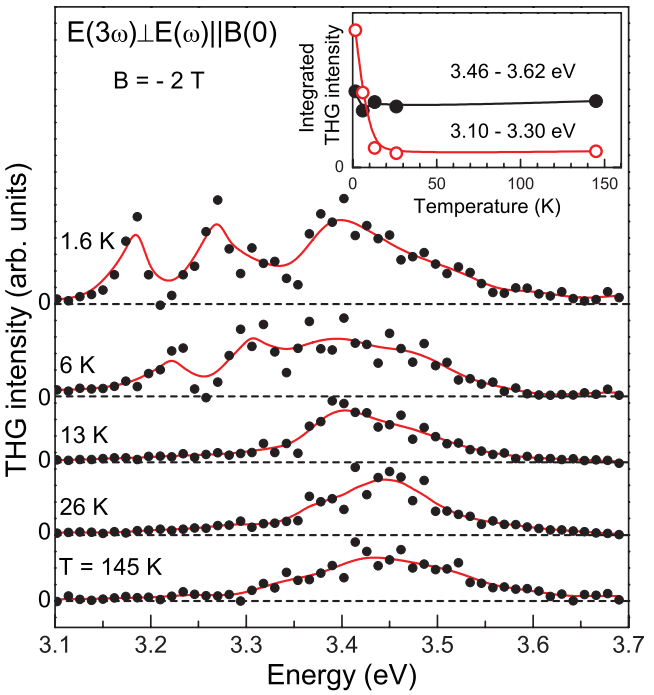

FIG. 5. (Color online) THG spectra of EuSe in the range 3.1–3.7 eV measured at different temperatures. Solid lines give a guide for the eye and dashed lines indicate zero level. The inset shows the temperature dependence of THG intensity integrated over two spectral ranges.

the THG signal intensity at energies exceeding 3.4 eV are quite stable against temperature increase up to 145 K, which is characteristic for CED contribution; compare with the inset of Fig. 1. This behavior is quantified in more detail in the inset of Fig. 5, where the temperature dependencies of the THG intensity integrated over two spectral range 3.1–3.3 eV and 3.45–3.6 eV are shown. It therefore becomes clear that

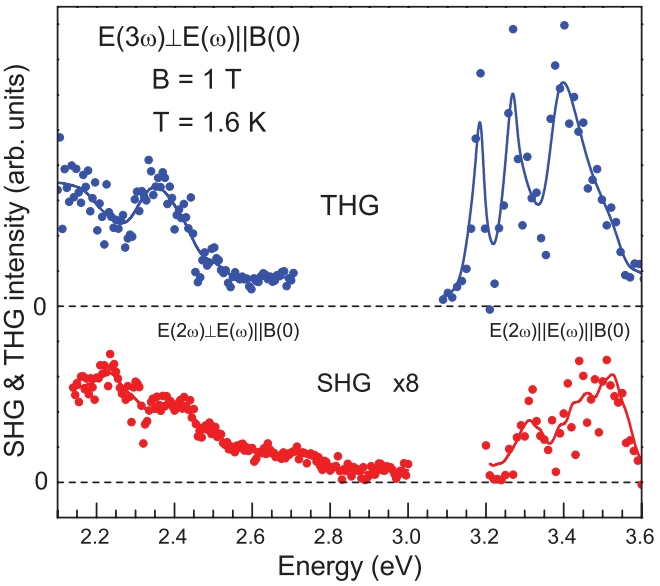

FIG. 6. (Color online) Comparison of magnetic-field-induced THG and SHG spectra of EuSe. Solid lines give a guide for the eye and dashed lines indicate zero level. SHG spectrum is multiplied by a factor of 8 for better visibility.

temperature variation is a very valuable tool for separating CED and IED contributions in THG spectra.

It is instructive to compare THG and SHG signals induced by an external magnetic field. Such comparison for a wide spectral range is presented in Fig. 6 for $B = 1$ T. Most of the experimental data are shown for the $\mathbf{E}(3\omega,2\omega) \perp \mathbf{E}(\omega)||\mathbf{B}(0)$ configuration, while the SHG signal in the spectral range 3.2–3.6 eV is detectable only in the $\mathbf{E}(2\omega)||\mathbf{E}(\omega)||\mathbf{B}(0)$ configuration. The good agreement in energy positions of observed bands in the THG and SHG spectra confirms that the origin of the both processes is related to the electronic structure of EuSe. However, the intensity of the THG signal is much stronger than that of the SHG signal. Such a behavior has been already reported for EuTe.[21] The fact that in Eu*X* the magnetic-field-induced THG process is of the electric-dipole type but the SHG process is attributed to nonlinearities of the magnetic-dipole type[19,20] explains why SHG and THG intensities differ so much in magnitude.

V. CONCLUSIONS

We have shown that particular features of the crystallographic structure and the electronic band structure of the centrosymmetric EuSe allow crystallographic and magnetic-field-induced third harmonics generation. We have studied THG spectra and observed several resonances in the vicinity of the band gap at 2.1–2.6 eV and at higher energies up to 3.7 eV. In contrast to the SHG studies,[19,20,39] the electric-dipole-type THG signal was found at zero magnetic field. The observed resonances were assigned to electronic transitions of Eu^{2+} ions involving the ground $4f^7$ states at the top of the valence band and excited $4f^6 5d^1$ states, which form the conduction band in EuSe. Strong resonant magnetic-field-induced THG signals at 2.1–2.6 eV and 3.1–3.7 eV were assigned to the $5d(t_{2g})$ and $5d(e_g)$ bands, respectively. This is qualitatively similar to the THG spectrum seen in EuTe, but the $e_g - t_{2g}$ emissions are more widely separated in EuSe than in EuTe, because of the larger $5d$ crystal-field splitting in EuSe. Temperature, magnetic-field, and rotational anisotropy studies allowed us to distinguish between crystallographic and magnetic-field-induced contributions to the THG signals. A strong modification of the THG intensity was observed in applied magnetic fields at particular resonances due to interference of crystallographic and magnetic-field-induced contributions. The magnetic-field dependence of the THG spectrum reflects the complicated magnetic phase diagram of EuSe, and THG intensity steps could be seen at the boundary between AFM, FIM, and FM orderings. We foresee that THG spectroscopy can be extended to other centrosymmetric magnetic bulk semiconductors and insulators, as well as to thin films and artificial structures, where SHG processes of electric-dipole type are forbidden, but ED THG processes are allowed.

ACKNOWLEDGMENTS

This work was supported by the Deutsche Forschungsgemeinschaft (Grant No. YA65/4-1), the Russian Foundation for Basic Research (Grant No. 10-02-01008), Russian Academy Programs on Spintronics, Physics of Nanostructures, and Quantum Physics of Condensed Matter, FoNE of the European Science Foundation, the Brazilian Agencies FAPESP and CNPq, the Deutscher Akademischer Austauschdienst (DAAD), and the FWF (I80-N20, Vienna, Austria).

[1] P. Wachter, *Handbook on the Physics and Chemistry of Rare Earths*, edited by K. A. Gschneider and L. R. Eyring (North-Holland, Amsterdam, 1979), Vol. 11, p. 507.

[2] G. Güntherodt, Phys. Condens. Matter **18**, 37 (1974).

[3] E. L. Nagaev, *Physics of Magnetic Semiconductors* (Mir, Moscow, 1983).

[4] J. Lettieri, V. Vaithyanathan, S. K. Eah, J. Stephens, V. Sih, D. D. Awschalom, J. Levy, and D. G. Schlom, Appl. Phys. Lett. **83**, 975 (2003).

[5] A. Schmehl, V. Vaithyanathan, A. Herrnberger, S. Thiel, C. Richter, M. Liberati, T. Heeg, M. Röckerath, L. F. Kourkoutis, S. Mühlbauer, P. Böni, D. A. Muller, Y. Barash, J. Schubert, Y. Idzerda, J. Mannhart, and D. G. Schlom, Nat. Mater. **6**, 882 (2007).

[6] P. G. Steeneken, L. H. Tjeng, I. Elfimov, G. A. Sawatzky, G. Ghiringhelli, N. B. Brookes, and D.-J. Huang, Phys. Rev. Lett. **88**, 047201 (2002).

[7] T. S. Santos and J. S. Moodera, Phys. Rev. B **69**, 241203 (2004).

[8] T. S. Santos, J. S. Moodera, K. V. Raman, E. Negusse, J. Holroyd, J. Dvorak, M. Liberati, Y. U. Idzerda, and E. Arenholz, Phys. Rev. Lett. **101**, 147201 (2008).

[9] G.-X. Miao, M. Müller, and J. S. Moodera, Phys. Rev. Lett. **102**, 076601 (2009).

[10] G. Springholz, A. Raab, R. T. Lechner, and V. Holy, Appl. Phys. Lett. **79**, 1225 (2001).

[11] J. S. Moodera, X. Hao, G. A. Gibson, and R. Meservey, Phys. Rev. Lett. **61**, 637 (1988).

[12] X. Hao, J. S. Moodera, and R. Meservey, Phys. Rev. B **42**, 8235 (1990).

[13] A. T. Filip, P. LeClair, C. J. P. Smits, J. T. Kohlhepp, H. J. M. Swagten, B. Koopmans, and W. J. M. de Jonge, Appl. Phys. Lett. **81**, 1815 (2002).

[14] P. LeClair, J. K. Ha, H. J. M. Swagten, J. T. Kohlhepp, C. H. V. de Vin, and W. J. M. de Jonge, Appl. Phys. Lett. **80**, 625 (2002).

[15] C. J. P. Smits, A. T. Filip, J. T. Kohlhepp, H. J. M. Swagten, B. Koopmans, and W. J. M. de Jonge, J. Appl. Phys. **95**, 7405 (2005).

[16] J. Trbovic, C. Ren, P. Xiong, and S. von Molnar, Appl. Phys. Lett. **87**, 082101 (2005).

[17] C. Ren, J. Trbovic, R. L. Kallaher, J. G. Braden, J. S. Parker, S. von Molnar, and P. Xiong, Phys. Rev. B **75**, 205208 (2007).

[18] J. S. Moodera, R. Meservey, and X. Hao, Phys. Rev. Lett. **70**, 853 (1993).

[19] B. Kaminski, M. Lafrentz, R. V. Pisarev, D. R. Yakovlev, V. V. Pavlov, V. A. Lukoshkin, A. B. Henriques, G. Springholz, G. Bauer, E. Abramof, P. H. O. Rappl, and M. Bayer, Phys. Rev. Lett. **103**, 057203 (2009).

[20]B. Kaminski, M. Lafrentz, R. V. Pisarev, D. R. Yakovlev, V. V. Pavlov, V. A. Lukoshkin, A. B. Henriques, G. Springholz, G. Bauer, E. Abramof, P. H. O. Rappl, and M. Bayer, Phys. Rev. B **81**, 155201 (2010).

[21]M. Lafrentz, D. Brunne, B. Kaminski, V. V. Pavlov, A. B. Henriques, R. V. Pisarev, D. R. Yakovlev, G. Springholz, G. Bauer, E. Abramof, P. H. O. Rappl, and M. Bayer, Phys. Rev. B **82**, 235206 (2010).

[22]M. Matsubara, A. Schmehl, J. Mannhart, D. G. Schlom, and M. Fiebig, Phys. Rev. B **81**, 214447 (2010).

[23]M. Matsubara, C. Becher, A. Schmehl, J. Mannhart, D. G. Schlom, and M. Fiebig, J. Appl. Phys. **109**, 07C309 (2011).

[24]M. Fiebig, V. V. Pavlov, and R. V. Pisarev, J. Opt. Soc. Am. **22**, 96 (2005).

[25]V. V. Pavlov, A. M. Kalashnikova, R. V. Pisarev, I. Sänger, D. R. Yakovlev, and M. Bayer, Phys. Rev. Lett. **94**, 157404 (2005).

[26]I. Sänger, D. R. Yakovlev, R. V. Pisarev, V. V. Pavlov, M. Bayer, G. Karczewski, T. Wojtowicz, and J. Kossut, Phys. Rev. Lett. **96**, 117211 (2006).

[27]R. T. Lechner, G. Springholz, T. U. Schülli, J. Stangl, T. Schwarzl, and G. Bauer, Phys. Rev. Lett. **94**, 157201 (2005).

[28]T. Kasuya, Crit. Rev. Solid State Mater. Sci. **3**, 131 (1972).

[29]T. Kasuya, IBM J. Res. Dev. **14**, 214 (1970).

[30]Y. R. Shen, *The Principles of Nonlinear Optics* (Wiley, New York, 1984).

[31]R. W. Boyd, *Nonlinear Optics* (Academic, San Diego, 1993).

[32]S. V. Popov, Y. P. Svirko, and N. I. Zheludev, *Susceptibility Tensors for Nonlinear Optics* (Institute of Physics Publishers, Philadelphia, 1995).

[33]R. R. Birss, *Symmetry and Magnetism* (North-Holland, Amsterdam, 1967).

[34]S. A. Akhmanov, V. I. Emel'yanov, N. I. Koroteev, and V. N. Seminogov, Sov. Phys. Usp. **28**, 1084 (1985).

[35]R.-P. Pan, H. D. Wei, and Y. R. Shen, Phys. Rev. B **39**, 1229 (1989).

[36]A. Mauger and C. Godart, Phys. Rep. **141**, 51 (1986).

[37]J. Schoenes and P. Wachter, Physica B **89**, 155 (1977).

[38]A. B. Henriques, A. Wierts, and M. A. Manfrini, G. Springholz, P. H. O. Rappl, E. Abramof, and A. Y. Ueta, Phys. Rev. B **72**, 155337 (2005).

[39]A. B. Henriques, E. Abramof, and P. H. O. Rappl, Phys. Rev. B **80**, 245206 (2009).